

The importance of strain-coupling in 2-2 composite structures: Determination of the local strain fields using a digital image correlation system

Alexander Martin^{1,2,*}, Juliana G. Maier¹, Friedemann Streich³, Marc Kamlah³, Kyle G. Webber¹

¹Department of Materials Science and Engineering, Friedrich-Alexander-Universität Erlangen-Nürnberg, Erlangen 91058, Germany

²Department of Life Science and Applied Chemistry, Graduate School of Engineering, Nagoya Institute of Technology, Nagoya 466-8555, Japan

³Institute for Applied Materials (IAM-WBM), Karlsruhe Institute of Technology, Eggenstein-Leopoldshafen 76344, Germany

*corresponding author: martin.alexander@nitech.ac.jp

Abstract

Ceramic-ceramic composite structures are a viable solution to improve the electromechanical response of lead-free ferroelectrics through tuning of the local electrical and mechanical fields. The origin of the enhanced properties, however, remains unclear, as many of the possible effects, such as polarization and strain coupling as well as interface diffusion, are interrelated and difficult to separate or directly investigate. In this study, we use a custom-built digital image correlation system to directly investigate the influence of strain coupling on 2-2 composites consisting of $0.90\text{Na}_{1/2}\text{Bi}_{1/2}\text{TiO}_3\text{-}0.06\text{BaTiO}_3\text{-}0.04\text{K}_{0.5}\text{Na}_{0.5}\text{NbO}_3$ (NBT-6BT-4KNN) and $0.94\text{Na}_{1/2}\text{Bi}_{1/2}\text{TiO}_3\text{-}0.06\text{BaTiO}_3$ (NBT-6BT) by varying the mechanical interface contacts between end members. Specifically, two model cases were utilized to separate the relative contributions of the polarization and strain coupling mechanisms: (i) electrically connected and (ii) mechanically and electrically connected. A digital image correlation (DIC) system was used to observe the local strain response of the different layers across the interface as well as the macroscopic large signal longitudinal and transverse ferroelectric response. Experimental results reveal an enhancement of the large signal piezoelectric coefficient d_{33}^* by approximately 10 % from 390 pm/V to 440 pm/V due to strain coupling.

1. Introduction

In order to replace lead-containing ferroelectric materials due to environmental and health concerns, a number of lead-free material systems have been identified, such as (K, Na) NbO₃ (KNN)-based¹, Na_{1/2}Bi_{1/2}TiO₃ (NBT)-based², and BaTiO₃ (BT)-based³ materials. Among them, the (Na_{1/2}Bi_{1/2})TiO₃-BaTiO₃ (NBT-BT) system, in particular in the vicinity of the morphotropic phase boundary (MPB) at a BT-content of approximately 6 ~ 7 mol% that separates the rhombohedral NBT and tetragonal BT phases⁴⁻⁶, has demonstrated exceptionally large unipolar strains that are of interest for actuation systems. Subsequently, Zhang *et al.* demonstrated a giant electric-field-induced strain through the introduction of an additional end member that was able to modulate the thermal stability of the nonergodic-ergodic relaxor transition through destabilization of the electrically induced long-range ferroelectric order.^{5 10,11}

NBT-BT near the MPB is a non-ergodic relaxor at room temperature, arising due to the lack of chemical order, which is supported by both analytical⁷⁻⁹ and experimental⁸⁻¹⁶ investigations. This chemical heterogeneity can result in the formation of local polar nanoregions (PNRs), which are embedded in a nonpolar matrix. TEM observations by Cheng *et al.*^{17,18} have found a core-shell structure consisting of a nanosized tetragonal core embedded in a cubic shell in (Na_{1/2}Bi_{1/2})TiO₃-0.026BaTiO₃-0.12(Bi_{0.5}K_{0.5})TiO₃. Despite this local perovskite structure, *in situ* diffraction studies have demonstrated that NBT-7BT lacks a long-range ferroelectric order in the virgin state typical of perovskite ferroelectrics¹⁹. However, during the application of an electric field, a field-induced transformation to a meta-stable lower-symmetry phase is observed¹⁹, corresponding to the formation of metastable

ferroelectric domains^{5,6,20,21} and the development of a large polarization and strain response. This is understood to be a field-induced transition from the relaxor state to a metastable long-range ferroelectric order. With increasing temperature, however, the metastable ferroelectric order can be thermally destabilized. In the vicinity of the critical temperature T_{F-R} , which is separating the ergodic and non-ergodic relaxor states^{22,23}, the remanent polarization and strain is reduced through the loss of metastability and the spontaneous transition back to the macroscopic non-polar state during removal of the electric field.^{23,24} Through the reversibility of the electric-field induced phase transformation, large differences between maximum and remanent polarization and strain are achieved, resulting in a large electromechanical response. Importantly, the metastability of the long-range ferroelectric order can be chemically tuned using relatively small amounts of various end members. For example, Zhang et al. in 2007² modified the NBT-BT system with KNN forming the solid solution $(\text{Na}_{1/2}\text{Bi}_{1/2})\text{TiO}_3\text{-BaTiO}_3\text{-(K}_{0.5}\text{Na}_{0.5})\text{NbO}_3$ (NBT-BT-KNN), effectively shifting the T_{F-R} to room temperature and resulting in large electric-field-induced strains of up to 0.45 %.²³

Despite the potential of ergodic relaxor materials, the relatively large electric fields required to induce long-range ferroelectric order as well as the significant hysteresis limit their potential integration into applications. Thus, an important goal is to reduce the critical electric field required to induce long-range ferroelectric order, referred to as the poling field E_{pol} , while maintaining a large strain. One proposed method to reduce the poling field is through the development of ceramic-ceramic composites, which has been previously investigated by Dausch et al. for lead-based ferroelectric-antiferroelectric (FE-AFE) composites^{25,26}. They observed a reduction of the required electric field for the phase transition from AFE to FE by the presence of FE phase in an AFE matrix, where the critical electric field as a function of FE content was estimated by using a two-serially-connected capacitor model. In this case, the polarizations in the capacitors were assumed to be coupled, meaning that the macroscopic electrical response of the capacitors influence one another. As both end members showed different macroscopic polarization-electric field responses, there was assumed to be a local redistribution of the applied electric field that caused a shift in the apparent critical field in the AFE component.^{27,28} This work, however, did not take the effect of strain coupling into account, where the mechanical interaction of the components can influence the electromechanical response. Subsequently, Lee et al.^{27,28} showed an enhancement in the large field strain behavior for lead-free relaxor (RE)/ ferroelectric (FE) 0-3 type composites (phase assembly nomenclature by Newnham²⁹), demonstrating that the composite structure not only provides a reduction of the driving electric field but also yields an enhanced strain by tailoring the contents of the RE and FE phases. Later, Groh et al. showed similar results for $0.92(\text{Na}_{1/2}\text{Bi}_{1/2})\text{TiO}_3\text{-}0.06\text{BaTiO}_3\text{-}0.02\text{K}_{0.5}\text{Na}_{0.5}\text{NbO}_3$ and $0.93\text{NBT}\text{-}0.07\text{BT}$ (NBT-7BT) composites.^{30,31} Despite these promising results, the underlying mechanisms are still not fully understood, such as the internal residual stresses arising from different sintering trajectories of the end members, interdiffusion between the constituents, the influence of strain coupling, etc. For this reason, studies on 2-2 composites have been conducted on different material systems to highlight certain aspects³²⁻³⁵. In particular, the work by Zhang et al.³⁵ showed the importance of strain-coupling in multilayer composites of $0.91(\text{Na}_{1/2}\text{Bi}_{1/2})\text{TiO}_3\text{-}0.06\text{BaTiO}_3\text{-}0.03\text{AgNbO}_3$ and NBT-7BT by varying the orientation of the interfaces parallel and perpendicular to the applied electric field, where it was possible to remove the influence of the polarization coupling. As a result, improvements of the electromechanical properties of the constituents were observed only for the strain-coupled samples, showing the influence of mechanical-coupling in addition to polarization coupling. Similar conclusions were reached by Ayrikyan et al.³⁴ in two separate composite systems. For one NBT-7BT was combined with $(\text{Na}_{1/2}\text{Bi}_{1/2})\text{TiO}_3\text{-}25\text{SrTiO}_3$, where the enhancement could not only be attributed to polarization coupling, but also to strain coupling between the constituents. Further studies also showed that the interdiffusion between the constituent materials can change with the volume fraction of the seed material, as well as the stresses during sintering and the resulting residual stress. These changes at the interface can have an overall impact on the composite, as it changes the mechanical properties around the interface, together with increased pore fraction, increased grain size, and changes to the crystallographic structure^{32,33}. For instance, as pores have a relative permittivity of 1, charge accumulation during the application of an electric field can occur at the interface between the pore and the ferroelectric, resulting in a localized large electric field. As a result, the bilayer composition of NBT-7BT with 20 vol% $0.94\text{Bi}_{0.5}(\text{Na}_{0.75}\text{K}_{0.25})0.5\text{TiO}_3\text{-}0.06\text{BiAlO}_3$ showed the highest increase in pore size and therefore also the highest strain response as shown by Ayrikyan³².

To date, strain measurements on such composites were performed by using techniques that capture the average strain response of the entire composite and ignore the inherent inhomogeneous strain fields observed through the

composite structure. This is especially true for observations near the interface, which is separating the constituent members, thereby limiting the understanding of the mechanisms responsible for the electromechanical coupling in ceramic-ceramic composites. Here, the digital image correlation (DIC) method can directly provide full-field displacements to sub-pixel accuracy and full-field strains by comparing the digital images of a test object surface acquired before and after deformation^{36,37}. The DIC method allows for the direct investigation of a region of interest on a test object surface, making this technique a highly effective tool suitable for monitoring the local deformations in ceramic-ceramic composites. In this work, NBT-6BT-4KNN and NBT-6BT were used as RE and FE materials, respectively. 2-2 RE/FE bilayer composites with varying RE and FE volume fractions were prepared to directly investigate the polarization and strain coupling effects by modifying the electrical and mechanical boundary conditions of the composites. The DIC method was used to study the local strain fields of each layer of the RE/FE multilayer composite as well as the interface region during electric field loading.

2. Experimental methodology

NBT-6BT-4KNN and NBT-6BT powders were produced via solid oxide synthesis route and chosen for relaxor and ferroelectric material for the bilayer structure, respectively. The used starting powders were Bi₂O₃ (99.975 % purity, Alfa Aesar), TiO₂ (99.6 % purity, Alfa Aesar), Na₂CO₃ (99.95 % purity, Alfa Aesar), K₂CO₃ (99.95 % purity, Alfa Aesar), Nb₂O₅ (99.95 % purity, Alfa Aesar), and BaCO₃ (99.95 % purity, Alfa Aesar). The powders were mixed according to their stoichiometric formula and milled together with ZrO₂ balls in ethanol for 24 h, followed by calcination at 800 °C for 2 h. The final powders were uniaxially pressed and subsequently cold-isostatically pressed at -180 MPa. Afterwards, the green bodies were sintered at 1150 °C for 3 h using powder of same composition for sacrificial purposes, where the heating and cooling rates were 3 K/min and 3 K/min, respectively. Samples were cut and ground to rectangular samples with a surface area of 4 mm x 4 mm using a surface grinder. In order to produce bilayers with varying volume fractions of the RE and FE end members, the height of the individual components was adjusted accordingly, where the total height of the bilayer was fixed to 4 mm. During this investigation, bilayers with a volume ratio 0, 50, and 100 vol% seed were measured. The surfaces of the samples were sputtered with gold to create electrodes and the samples were annealed at 500 °C for 1 h in order to reduce internal stresses and stress-induced ferroelectric phases that occurred during sample preparation.

During electrical testing, two different cases were used: case (i), where the samples were stacked with a series electrical connection but without a mechanical connection, assuming to lead to only polarization coupling (PC) and case (ii), where both layers were electrically connected in series and also mechanically joined by gluing via silver paste, assuming to lead to polarization and strain coupling (PSC). It is important to note that the effects of friction in case (i) were assumed to be negligible, meaning that the samples were assumed to independently deform without mechanical constraints from the measurement system or the adjoining sample. In order to measure the electromechanical responses of the bilayer samples, the measurement setup as shown schematically in Figure 1 was used, which was comprised of a Sawyer-Tower circuit with a reference capacitor C_{ref} of 4.9 nF to measure the electric field dependent polarization as well as a linear variable differential transformer (LVDT) to record the total strain of the bilayers. Electric fields with a triangular waveform using a maximum value of ± 4 kV/mm and a loading rate of 0.08 kV/mm s⁻¹ (0.1 Hz) were applied parallel to the 3-direction with a high-voltage power supply (Trek Amplifier, Model 20/20C); a custom-built LabVIEW program was used as a waveform generator and a data recording and analysis program for the polarization and LVDT strain measurements. Importantly, measurements were started from the virgin, unpoled state, providing information on the remanent strain development during electric field loading.

In order to directly observe the electromechanical response of the different layers, a digital camera (MC089MG-SY-UB, Ximea GmbH) with a resolution of 4112 x 2176 pixels that imaged one side of the sample for the DIC system was used. Combined with a lens with 2x magnification (MVO-TML Telecentric Measuring Lens, Edmund Optics Inc.) a resolution of 1.75 μ m/pixel could be achieved. Artificial speckles were sprayed onto the observation surfaces by means of an air brush (AT-Airbrush Pistole Kit, AT-AK-02, Agora-Tec), thus allowing the creation of patterns suitable for DIC tracking. The camera captured 2 images per second to record the deformation during electric field loading. The images were analyzed using a commercially available DIC-program, VedDAC (Version 6.0). Here, a distance of 60 pixel or 105 μ m between the measurement points as well as a reference field of 120 x 120 pixel were used. Additionally, the hair wavelet function was chosen to increase accuracy and minimize the

standard deviation between points. Using this technique, the strain field was characterized as a function of position through the thickness of the sample by averaging the strain values along a line parallel to the interface. To measure the noise, images of the sample were taken for 100 s without the application of an electric field while using the same DIC parameters. A background noise level of 0.04 pixels or approximately 0.002 % was observed.

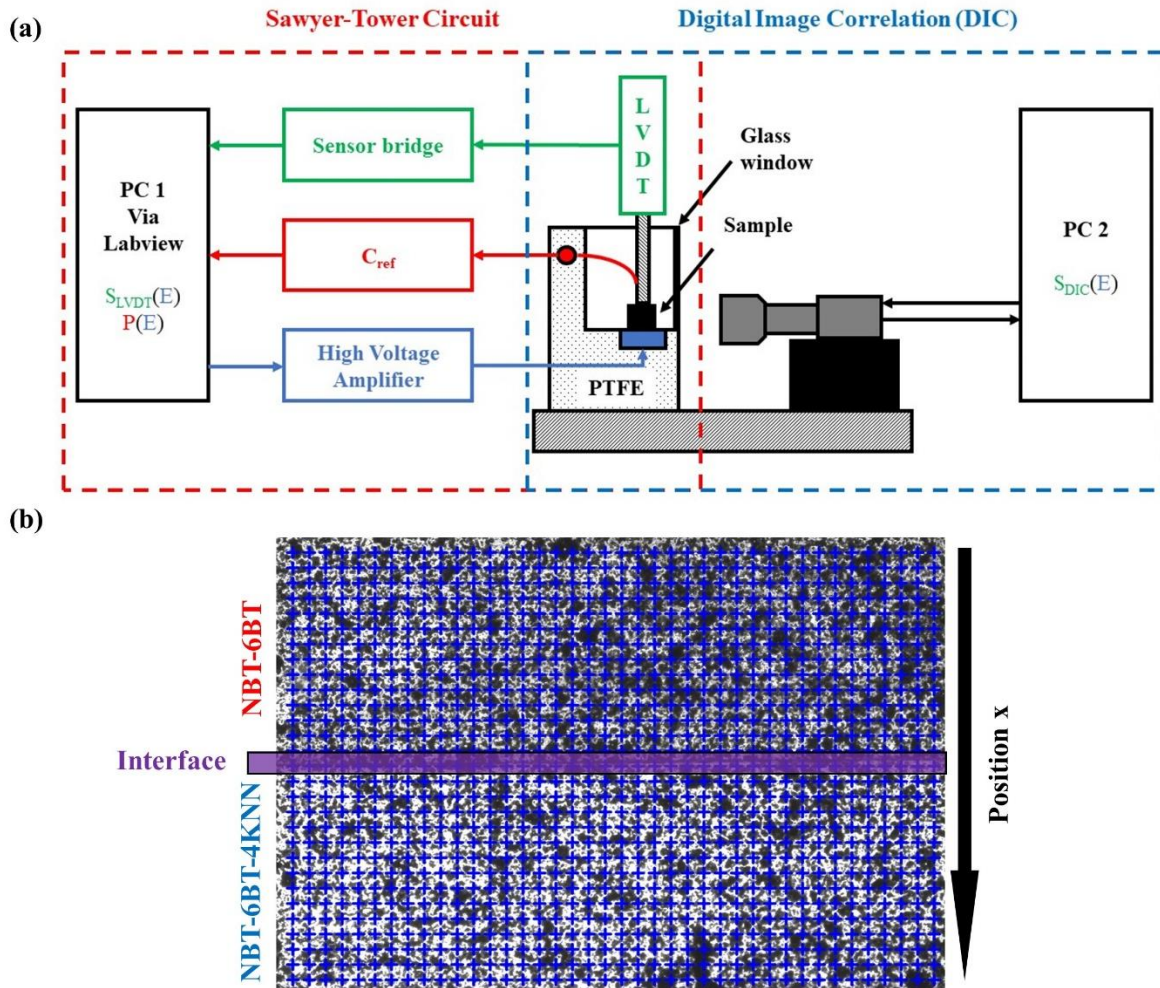


Figure 1. Schematics of the experimental setup, which combines overall polarization and strain measurements with spatial resolution of the strain via DIC (a). The amount of measurement points across the bilayer sample, as used during the DIC measurement (b)

3. Results and discussion

The DIC measurement system was used to characterize the macroscopic longitudinal and transverse strain response of the end members NBT-6BT and NBT-6BT-4KNN as well as their ceramic-ceramic composites with both PC and PSC connectivity (Fig. 2). It is important to note that slight differences can occur due to changes in lighting during measurement, from e.g., minor vibrations or silicone oil movement, that can affect the images used for DIC analysis. In particular, silicone oil, which was used as an electrical insulating liquid during the high voltage experiments, was found to move during the application of an electric field, resulting in minor variations of the light exposure from image to image that increased error. This error was minimized by locating the sample as close as possible to the glass window to reduce the volume of silicone oil between the sample surface and the camera and limiting the electrical loading frequency. Importantly, despite the increased local error in the determination of strain fields, the average value of a larger region was found to provide accurate strain results. To ensure accuracy of the strain results from the DIC analysis, they were directly compared to longitudinal strain measurements from an LVDT, where an excellent agreement is observed (Fig. 2).

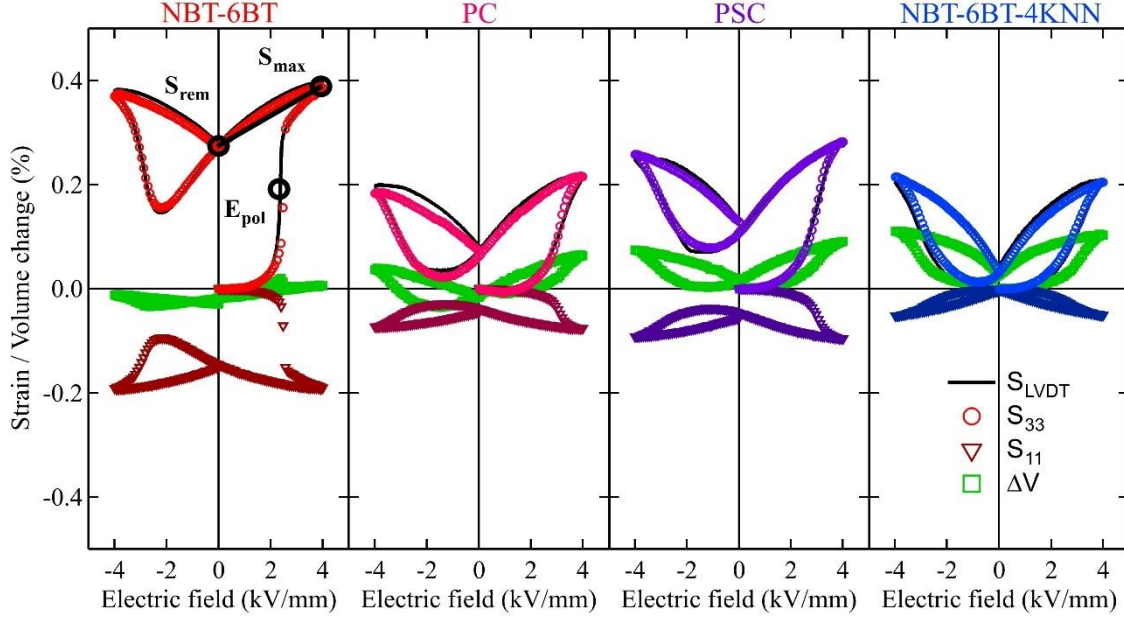


Figure 2. The longitudinal strain (S_{33}) and transverse strain (S_{11}) as well as the resulting volumetric strain (ΔV) as a function of electric field for NBT-6BT, PC, PSC, and NBT-6BT-4KNN. The longitudinal strain data determined with the DIC system was compared to an LVDT, shown as a black line, indicating close correlation between both measurement methods.

NBT-6BT shows a typical non-ergodic relaxor strain-electric field hysteresis response with a large remanent ($S_{rem} = 0.25\%$) and maximum strain ($S_{max} = 0.36\%$). To calculate the large signal piezoelectric coefficient d_{33}^* and d_{31}^* , the maximum and remanent strain were subtracted and divided by the maximum electric field ($S_{max} - S_{rem}/E_{max}$), which was 4 kV/mm for each case. In addition, for the d_{33}^* the longitudinal strain (S_{33}), and for d_{31}^* the transverse strain (S_{11}) was used. This resulted in a d_{33}^* and d_{31}^* of approximately 250 pm/V and -112 pm/V for NBT-6BT, respectively. In addition, during initial electric field loading from the virgin state, a significant jump in longitudinal and transverse strain is observed at the poling field ($E_{pol} = 2.3$ kV/mm), defined as the inflection point during the first increase of the electric field and describes the critical electric field to induce a transition from the relaxor state to long-range ferroelectric order. In contrast, NBT-6BT-4KNN did not display a significant remanent strain development (0.05%). However, due to this and the relative high observed maximum strain ($S_{max} = 0.21\%$), the large signal piezoelectric coefficient was found to be nearly 56% larger than for NBT-6BT ($d_{33}^* = 390$ pm/V, $d_{31}^* = -120$ pm/V). The poling field for NBT-6BT-4KNN was found to be 2.7 kV/mm.

Importantly, the DIC method also allows the simultaneous characterization of the strain perpendicular to the applied electric field (S_{11}), which is also shown in Figure 2. In all cases, the transverse strain mirrors the form of the longitudinal strain (S_{33}), where the magnitude is approximately half the longitudinal value for NBT-6BT and a fourth for NBT-6BT-4KNN. By combining the strain components, S_{33} and S_{11} , it is possible to directly characterize the volume change during electric field loading³⁸, assuming a transversely isotropic electromechanical response:

$$\Delta V \cong S_{33} + 2S_{11} \quad (1)$$

During the application of an electric field, changes in, e.g., the crystal symmetry, domain state, or defect network result in the formation of local strains. Importantly, some of these effects are volume conserving, such as domain wall motion³⁹, whereas others, such as field induced structural phase transitions, can be driven by changes in volume⁴⁰. It is important to note, however, that although field induced structural phase transitions can also be induced by deviatoric stress components, e.g. in potassium bicarbonate (KHCO_3)⁴¹, such structural transitions are understood to be coupled to a change in volume between crystal phases in perovskite ferroelectric oxides. In relaxor ferroelectrics undergoing either a reversible or irreversible field induced phase transformation to long-

range ferroelectric order, previous studies have shown that remanent volume changes can occur in NBT-BT compositions that are related to the coalescence of nano-polar regions³⁸. In this study, NBT-6BT does not show significant volume change, suggesting that the transformation involves no crystallographic symmetry change. These results are consistent with the work of Jo *et al.*³⁸, who measured the volume change of NBT-BT with changing BT content. In contrast, NBT-6BT-4KNN displays a maximum volume expansion of approximately 0.1 %, indicating the presence of a field-induced phase transformation.

Interestingly, the composite samples in Figure 2 show a strain response between the end members, in terms of the maximum and remanent strain as well as the critical poling field, which was found to depend on the mechanical coupling. For the electrically connected sample (PC), where both components were able to freely move without mechanical constraint, a remanent and maximum strain of 0.07 % and 0.20 % were observed, respectively. Importantly, assuming a simple rule of mixtures, a remanent strain of 0.15 % would be expected, nearly twice that observed experimentally. Similarly, the poling field ($E_{pol} = 3.3$ kV/mm) was larger than that found in both end members, which suggests that the effective local electric field distribution required an increase in the externally applied electric field to induce the formation of a long-range order. These differences in applied and effective electric field seem to lead to an overall decrease of electromechanical properties, resulting in a d_{33}^* of 310 pm/V and a d_{31}^* of -100 pm/V.

When the end members are mechanically connected through a conductive interface (PSC), there is the formation of a strain coupling during electrical activation through the large signal d_{31}^* piezoelectric coefficient that can influence the electromechanical response of the composite. In this case, an increased maximum ($S_{max} = 0.28$ %), and remanent strain ($S_{rem} = 0.11$ %) as well as a decreased poling field ($E_{pol} = 2.6$ kV/mm) were observed compared to the electrically connected sample. This resulted in an increased d_{33}^* of 440 pm/V, as well as an increased d_{31}^* of -128 pm/V. Both values show an enhancement of approximately 10 % compared to NBT-6BT-4KNN, which had the highest values in between the end members. These results are consistent with the literature for 0-3 composites. As shown by Groh *et al.*, NBT-BT/NBT-BT-KNN composites showed improved electromechanical behavior ($d_{33}^* = 500$ pm/V) at 50 vol.% NBT-6BT. It is important to note, however, that in addition to differences in end member connectivity, the samples in Groh *et al.* were co-sintered, thus interdiffusion as well as internal stresses due to differences in the sintering behavior and coefficients of thermal expansion can also play an important role. Nevertheless, these results suggested a strong influence of strain coupling on the overall properties of the composite.

In addition to mechanical interactions, both end members are electrically connected through the polarization coupling effect, which, due to variations in the dielectric permittivity, electrical resistance, and large field polarization response, can affect the local distribution of the externally applied electric field. Figure 3 shows representative polarization-electric field hysteresis curves for the end members as well as the PC and PSC bilayer composites. The matrix material NBT-6BT-4KNN displays a pinching behavior, typical for ergodic relaxor ferroelectrics,^{30,42,43} corresponding to low remanent polarization ($P_{rem} = 15$ $\mu\text{C}/\text{cm}^2$) and strain. In contrast, the seed material NBT-6BT, a nonergodic relaxor, shows no apparent pinching effect and the formation of a large remanent polarization ($P_{rem} = 43$ $\mu\text{C}/\text{cm}^2$), characteristic for this system⁴⁴. As such, the remanent polarization of the composite ($P_{rem} = 20$ $\mu\text{C}/\text{cm}^2$) increased with the addition of a nonergodic relaxor component, similar to previous studies^{28,30}. This behavior is to be expected, as NBT-6BT has higher remanent and maximum polarization. Interestingly, both the PC and PSC cases display a similar polarization behavior, in contrast to the strain-response, which shows a significantly higher remanent strain for the PSC sample. This is suggested to be due to the strain coupling between end members, where the increased mechanical connectivity affected the macroscopic constitutive response.

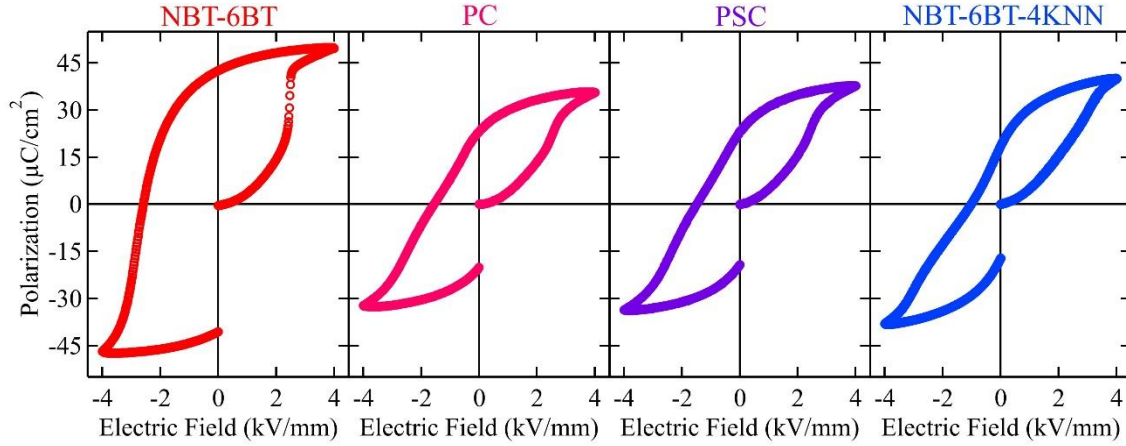


Figure 3: Results of polarization as a function of electrical field for NBT-6BT and NBT-6BT-4KNN, as well as the PC and PSC case.

When combining two capacitors in series, the charge and by extension the polarization for both capacitors must be equal, assuming infinite resistivity. In a system where the dielectric permittivity varies between each component, the local voltage on each capacitor is different and as a result, there is an inhomogeneous electric field distribution. To ensure equal polarization, an enhanced local electric field would be required in the NBT-6BT-4KNN layer, as NBT-6BT displays a larger polarization, which is expected to promote the electric field induced long-range ferroelectric order in the ergodic relaxor component at lower external electric fields. This has been used in different investigations to increase the effective electric field in relaxor-based composites^{27,28,30,31}. Using these results and combining them with the uncoupled results of the NBT-6BT end member (Figure 2), one could assume that NBT-6BT was not fully polarized during the measurement. This is suggested by the lower maximum and remanent polarization, as well as the higher poling field in the composite structure. In the PC case, it seemed the effective electric field on NBT-6BT was insufficient to polarize the sample and caused a significant increase in the polarization. As such, there was no significant increase in the electric field in NBT-6BT-4KNN and the electromechanical properties. This appeared to have been the case in PSC as well, however one would need to observe each layer individually to fully verify this. As such, the DIC method was used to directly investigate the strain response for each component, thus allowing for more information about the influence of strain coupling on the local properties.

The local strain-electric field behavior for NBT-6BT and NBT-6BT-4KNN are presented in Figure 4 for both the PC and PSC cases. Overall, the strain response for both end members change significantly when combining them in the ceramic-ceramic composite structures. In the case of NBT-6BT there is a decrease in the longitudinal remanent strain in both the PC and PSC configurations from 0.25 % to approximately 0.11 % and 0.10 %, respectively. Alongside the decrease in the maximum strain of the PC (S_{33}) composites, a reduction of the electromechanical properties of NBT-6BT ($d_{33}^* = 170$ pm/V, $d_{31}^* = -87$ pm/V) was observed. Interestingly, despite the decrease in the maximum strain of the PSC composites (S_{33}), almost no reduction in the PSC-case ($d_{33}^* = 235$ pm/V, $d_{31}^* = -117$ pm/V) occurred. It is important to note, that due to the redistribution of the applied electric field on the composite components, there was an apparent increase in the poling field of the PC sample to $E_{pol} = 3.3$ kV/mm. This is approximately 43 % higher than that observed for NBT-6BT ($E_{pol} = 2.3$ kV/mm), resulting in a lack of saturation of the longitudinal and transverse strain (Fig. 4b). This is understood to be the origin of the reduced electromechanical response in the NBT-6BT end member of the PC sample. Interestingly, mechanical coupling in the PSC sample was found to decrease the poling field ($E_{pol} = 2.6$ kV/mm) in comparison to polarization coupling alone to values comparable to that observed for the end member. Despite this, however, the remanent strain remained considerably lower compared to the uncoupled case, which is likely due to the mechanical constraints imposed by the NBT-6BT-4KNN layer.

Similarly, the local strain-electric field response of the NBT-6BT-4KNN layer was observed for both PC and PSC samples. NBT-6BT-4KNN is understood to be an ergodic relaxor at room temperature with a correspondingly low remanent strain, which is evident in the longitudinal and transverse strain behavior of the uncoupled sample (Fig. 4d). However, in both the PC and the PSC configuration there was an increase in the remanent and maximum

strain, hysteresis, and negative strain, defined as the strain difference between the lowest strain and the remanent strain as well as a corresponding change in the poling field. Changes in the remanent and negative strain are likely due to the formation of internal bias fields that can be developed during polarization coupling⁴⁵. Although residual mechanical fields could also affect the remanent state, in particular considering the large transverse remanent strain in the NBT-6BT end members, it is not expected to play a significant role, as similar remanent strains are observed in both PC and PSC samples despite the lack of mechanical coupling in the PC state. Similar to observations in NBT-6BT, the PC sample displayed an increase in the poling field over the end member from 2.7 kV/mm to 3.1 kV/mm, whereas the PSC sample decreased to 2.6 kV/mm. This resulted in a decrease in the electromechanical properties for the PC case ($d_{33}^* = 377$ pm/V, $d_{31}^* = -104$ pm/V) and an increase for the PSC case ($d_{33}^* = 490$ pm/V, $d_{31}^* = -124$ pm/V). These results clearly demonstrate the importance of strain coupling in enhancing the strain response of ceramic-ceramic composite structures.

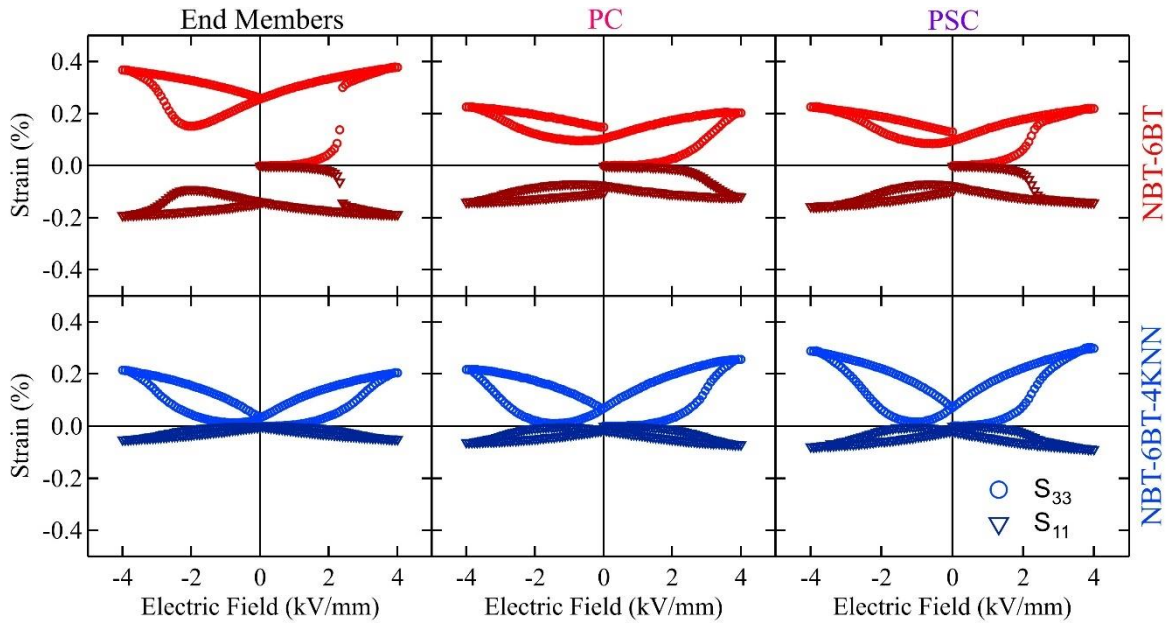


Figure 4. Strain-electric field hysteresis curves in longitudinal S_{33} and transverse S_{11} directions for end members NBT-6BT (a) and NBT-6BT-4KNN (d) as well as the NBT-6BT region in the PC and PSC configurations, (b) and (c), respectively, and the NBT-6BT-4KNN region in the PC and PSC configurations, (e) and (f), respectively. When testing individual regions, care was taken to remain at least 60 μm from the interface to ensure only the end member component of interest was investigated.

Interestingly, the composite structure was not found to significantly affect the poling field in either the NBT-6BT or the NBT-6BT-4KNN end members in the PSC sample. In order to investigate this, the strain difference between NBT-6BT and NBT-6BT-4KNN are measured from the virgin state as a function of the electric field for the PSC and PC cases, where the S_{11} strain difference between end member materials was determined ($\Delta S_{11} = S_{11,NBT-6BT} - S_{11,NBT-6BT-4KNN}$), providing information on the formation of internal biaxial stress during the application of an electric field. When comparing the values of the end members in the uncoupled case, up to 2 kV/mm, no significant change occurs, as both materials do not expand in that region. However, at 2 kV/mm NBT-6BT contracts sharply, resulting in a strain difference of approximately -0.14% . Interestingly, in the PC sample, the strain difference initially increases positively before decreasing sharply, suggesting that NBT-6BT-4KNN initially contracts before NBT-6BT. The reason hereby might be the change in the effective electric field, suggesting a larger effective electric field in NBT-6BT-4KNN and a lower effective electric field in NBT-6BT, when comparing to the non-composite case. Subsequently to this positive strain difference, however, the development of a large remanent strain in NBT-6BT and the corresponding transverse strain result in large strain gradient between end members above approximately 3 kV/mm. In the strain coupled case, no significant strain

difference was observed below 2 kV/mm, followed by a significant increase in the strain difference above 2 kV/mm. Considering the same effective electric fields as in the PC-case, this curve shows the strain coupling in effect. NBT-6BT-4KNN experiences a larger effective electric field compared to NBT-6BT, thus seems to contract before NBT-6BT, as suggested by the PC-curve. However, due to strain coupling, NBT-6BT contracts at first similar to NBT-6BT-4KNN, which is why the strain difference remains constant at 0 until approximately 2.3 kV/mm. Furthermore, the results suggest a lower poling field for NBT-6BT in the PSC case compared to the PC case, as the significant decrease in the strain difference occurs before the PC case. One possibility is due to biaxial compression on NBT-6BT, caused by the early contraction of NBT-6BT-4KNN as suggested by the PC case. The influence of biaxial/radial stress on the poling of ferroelectric materials has been previously reported, where a decrease in the poling field was observed^{46,47}. Nevertheless, it should be noted that the poling field in the PSC case is still higher than in the non-composite case, further proofing the lower effective electric field in NBT-6BT.

During the unloading phase, the PC case continues to increase in the strain difference from -0.01 % to -0.03 %. On the other hand, in the PSC case NBT-6BT, as well as NBT-6BT-4KNN, seem to expand at the same rate, thus an almost constant strain difference of -0.06 % between them remains. This is due to the way the end members are connected in each case. In the PC case, both end members can freely move without any constraints whereas in the PSC case they are mechanically connected. As such, in the PSC case, as long as there is no significant deviation between the electric-field induced strain in NBT-6BT and NBT-6BT-4KNN, strain coupling occurs and the strain difference remains constant. This was the case in the beginning of the application of the electric field as well as during unloading of the sample.

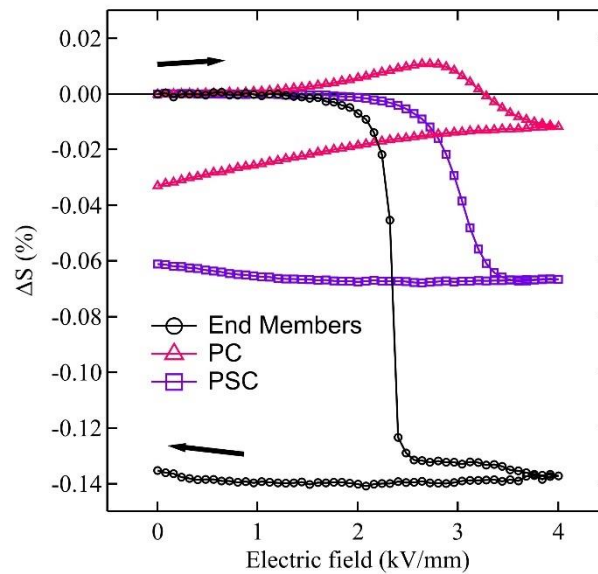


Figure 5: Strain difference between NBT-6BT and NBT-6BT-4KNN as a function of electric field.

In the initial, electrically unpoled state the internal residual stresses are zero, as each end member was combined at room temperature. However, during and following the application of an external electric field, the internal stress in the PSC composite will change depending on the transverse electromechanical response, including both the small signal transverse piezoelectric coefficient d_{31} as well as the macroscopic lateral strain d_{31}^* . In particular, the internal residual stresses remain once the electric field has been removed, as both end members display differences in transverse remanent strain. In order to demonstrate this effect, Figure 6 shows the strain as a function of the position through the cross-section of the composite structure for both the PC and the PSC cases. In the initially unpoled state, there is no strain gradient through the thickness of either configuration. However, with the application of an electric field, a significant increase in the strain gradient is observed. A sharp jump in strain is observed in the PC configuration when increasing the electric field over approximately 3.5 kV/mm, as no mechanical connection is present between the two end members. Importantly, however, the strain within each layer is uniform, displaying no significant gradient or variation within the resolution of the present measurements. This is the case for increasing the electric field as well as during decreasing. In contrast, the mechanical interface in the PSC case resulted in a more gradual, continuous strain transition through the thickness of the composite

structure. In particular, this is visible after unloading, where the NBT-6BT-4KNN sample shows a remanent strain close to the interface.

These data show that the strain gradient at the interface has a penetration depth into the end members of approximately 500 μm , after which a constant average strain is observed. Here, care was taken to select an appropriate reference field size for the DIC analysis. The reference field describes the size of the section at each measurement point, which will be searched via comparison to the subsequent images. The shift of this reference section thereby describes the displacement at that area. As such, if chosen too large, for example, the reference field would have gathered displacement information of the other material, resulting in an average value between the two, whereas too small would result in a larger error, as the reference field would contain less information for the comparison. Through experimentation, it is found that a reference field of 120 x 120 pixel or 204 x 204 μm resulted in reliable data. An additional possible source for error is the plastic deformation of the silver bond during the experiment. Using the DIC-results, a shear strain at the interface of about 0.18 % was calculated, which is in the elastic region for similar silver paste-based adhesives⁴⁸⁻⁵⁰. We therefore assume that the plastic deformation of the silver is minor. The results seem therefore to be a real effect caused by the strain coupling between the materials. *In situ* electric field dependent x-ray diffraction as a function of position would help to understand the relaxation process that leads to changes in the strain gradient with position.

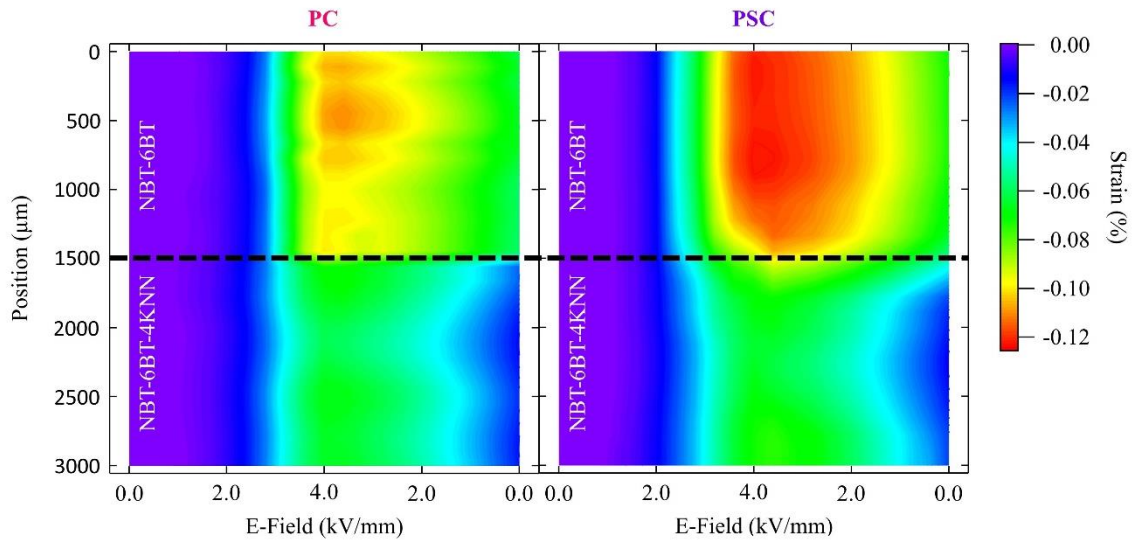


Figure 6: Strain as a function of position for the PC and PSC case for different electric field steps. The black line at 1500 μm signals the interface between NBT-6BT and NBT-6BT-4KNN.

At a sufficient distance to the interface, the strain is constant and describes bulk strain behavior of the constituent material. For the PSC sample, both materials show a deviation from this macroscopic strain behavior at the interface. As such, calculating the difference ($\Delta S = S_{11,0} - S_{11,x}$) between the average bulk strain $S_{11,0}$ and the strain at each position $S_{11,x}$, one can assume the mechanical stress via the elastic properties, such as the Young's modulus, at the interface. This difference in strain is shown in Figure 7 as a function of position across the interface. Closer to the interface the difference becomes negative for NBT-6BT-4KNN and positive for NBT-6BT. A positive ΔS suggests that the material contracted less at the interface than the normalized case, resulting in tensile stress. A negative ΔS on the other hand suggests a stronger contraction at the interface and by extension a compressive stress. In order to estimate the stresses, an isotropic, linear elastic response was assumed. The elastic modulus for NBT-6BT was found in previous investigations to be 105 GPa^{51,52}. For NBT-6BT-4KNN, however, the elastic modulus was assumed to be approximately 113 GPa⁵², based on values reported for NBT-6BT-2KNN. This variation in elastic properties would help to explain the larger strain difference in NBT-6BT, as a smaller elastic modulus would require a larger strain for force equilibrium. Using these elastic properties, a maximum residual stress of approximately 40 MPa was estimated at the interface. It should be noted that the residual stress could be quite different as a constant strain does not necessarily mean a stress-free region. Nevertheless, the results suggest that there is residual stress in the material and *in situ* x-ray diffraction through the layers could directly confirm the stress profile as well as the magnitude. Combined with the previous results, this residual stress is

responsible for the enhanced electromechanical properties^{46,47}. For instance, Kounga *et al.* have shown that through radial compressive stress assisted poling, a higher piezoelectric charge coefficient in PZT could be achieved. It should be mentioned that this improvement, however, was decreased after the mechanical load was removed, suggesting an improvement only by constant mechanical stress, which is the case in our setup. As such, NBT-6BT-4KNN showed higher piezoelectric properties in the PSC case ($d_{33}^* = 490$ pm/V) compared to the uncoupled sample ($d_{33}^* = 390$ pm/V). On the other hand, NBT-6BT, which is in tensile stress, showed an overall lower piezoelectric strain decreasing from initial 250 pm/V to 235 pm/V.

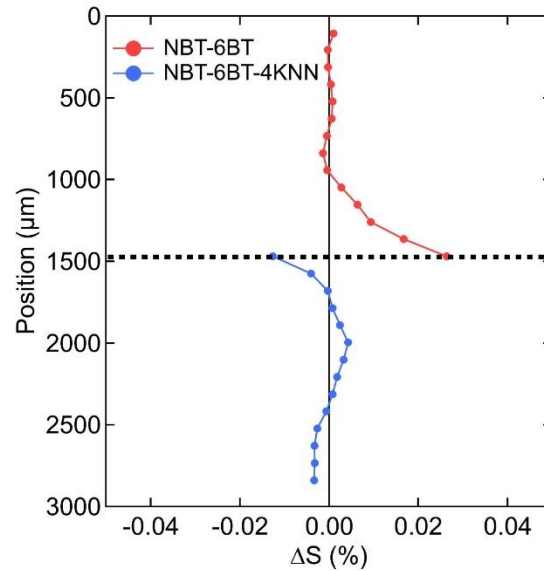


Figure 7: Strain difference between the constant strain and strain at interface as a function of position at an electric field E of 4 kV/mm in the PSC case. The black dotted line at 1500 μm represents the interface of the bilayer composite between NBT-6BT and NBT-6BT-4KNN.

Conclusion

The influence of electrical and mechanical interactions in bilayer composite structures of NBT-6BT and NBT-6BT-4KNN has been directly investigated using the DIC method. Experimental results indicate that polarization coupling alone does not result in an overall improvement of the electromechanical properties with the selected end members. However, with the addition of strain coupling between the layers, an overall enhancement of approximately 10 % was achieved. The DIC method, through *in situ* characterization of the local strain response of each end member, revealed that NBT-6BT was not fully polarized with only polarization coupling. As a result, high polarization values could not be achieved and the enhancement via polarization coupling was diminished. Through the introduction of mechanical coupling, however, the internal residual stresses developed due to the transverse electromechanical response induced a stress that enhanced the polarization of NBT-6BT. Subsequently, the sharp contraction of NBT-6BT results in a compressive stress in the NBT-6BT-4KNN layer that improves the longitudinal strain behavior.

Acknowledgements

The authors gratefully acknowledge financial support for this work by the Deutsche Forschungsgemeinschaft under WE 4972/5-1, KA 1019/14-1, and GRK2495/F.

References

- ¹ J.-F. Li, K. Wang, F.-Y. Zhu, L.-Q. Cheng, and F.-Z. Yao, *J. Am. Ceram. Soc.* **96**, 3677 (2013).
- ² S.T. Zhang, A.B. Kounga, E. Aulbach, H. Ehrenberg, and J. Rödel, *Appl. Phys. Lett.* **91**, 112906 (2007).
- ³ W. Liu and X. Ren, *Phys. Rev. Lett.* **103**, 257602 (2009).
- ⁴ T. Takenaka, K. Maruyama, and K. Sakata, *Jpn. J. Appl. Phys.* **30**, 2236 (1991).
- ⁵ G. Picht, J. Töpfer, and E. Hennig, *J. Eur. Ceram. Soc.* **30**, 3445 (2010).
- ⁶ C. Ma, H. Guo, S.P. Beckman, and X. Tan, *Phys. Rev. Lett.* **109**, 107602 (2012).
- ⁷ R. Pirc and R. Blinc, *Phys. Rev. B* **60**, 13470 (1999).
- ⁸ L.E. Cross, *Ferroelectrics* **76**, 241 (1987).
- ⁹ D. Viehland and L.E. Cross, *Phys. Rev. B* **43**, 8316 (1991).
- ¹⁰ D. Viehland, S.J. Jang, L.E. Cross, and M. Wuttig, *Phys. Rev. B* **46**, 8003 (1992).
- ¹¹ A. Naberezhnov, S. Vakhrushev, B. Dorner, D. Strauch, and H. Moudden, *Eur. Phys. J. B* **11**, 13 (1999).
- ¹² S.B. Vakhrushev and S.M. Shapiro, *Phys. Rev. B* **66**, 214101 (2002).
- ¹³ I.-K. Jeong, T.W. Darling, J.K. Lee, T. Proffen, R.H. Heffner, J.S. Park, K.S. Hong, W. Dmowski, and T. Egami, *Phys. Rev. Lett.* **94**, 147602 (2005).
- ¹⁴ N. Novak, R. Pirc, M. Wencka, and Z. Kutnjak, *Phys. Rev. Lett.* **109**, 1 (2012).
- ¹⁵ C.A. Randall, A.S. Bhalla, T.R. Shrout, and L.E. Cross, *J. Mater. Res.* **5**, 829 (1990).
- ¹⁶ P.M. Gehring, H. Hiraka, C. Stock, S.H. Lee, W. Chen, Z.G. Ye, S.B. Vakhrushev, and Z. Chowdhuri, *Phys. Rev. B - Condens. Matter Mater. Phys.* **79**, 24 (2009).
- ¹⁷ S.-Y. Cheng, J. Shieh, N.-J. Ho, and H.-Y. Lu, *Philos. Mag.* **91**, 4013 (2011).
- ¹⁸ S.Y. Cheng, J. Shieh, H.Y. Lu, C.Y. Shen, Y.C. Tang, and N.J. Ho, *J. Eur. Ceram. Soc.* **33**, 2141 (2013).
- ¹⁹ J.E. Daniels, W. Jo, J. Rödel, and J.L. Jones, *Appl. Phys. Lett.* **95**, 032904 (2009).
- ²⁰ L.A. Schmitt, J. Kling, M. Hinterstein, M. Hoelzel, W. Jo, H.-J. Kleebe, and H. Fuess, *J. Mater. Sci.* **46**, 4368 (2011).
- ²¹ R. Garg, B.N. Rao, A. Senyshyn, P.S.R. Krishna, and R. Ranjan, *Phys. Rev. B - Condens. Matter Mater. Phys.* **88**, 014103 (2013).
- ²² H. Foronda, M. Deluca, E. Aksel, J.S. Forrester, and J.L. Jones, *Mater. Lett.* **115**, 132 (2014).
- ²³ W. Jo, R. Dittmer, M. Acosta, J. Zang, C. Groh, E. Sapper, K. Wang, and J. Rödel, *J. Electroceramics* **29**, 71 (2012).
- ²⁴ W. Jo, T. Granzow, E. Aulbach, J. Rödel, and D. Damjanovic, *J. Appl. Phys.* **105**, 094102 (2009).
- ²⁵ D.E. Dausch, E. Furman, F. Wang, and G.H. Haertling, *Ferroelectrics* **177**, 221 (1996).
- ²⁶ D.E. Dausch, E. Furman, F. Wang, and G.H. Haertling, *Ferroelectrics* **177**, 237 (1996).
- ²⁷ D.S. Lee, D.H. Lim, M.S. Kim, K.H. Kim, and S.J. Jeong, *Appl. Phys. Lett.* **99**, 062906 (2011).
- ²⁸ D. Su Lee, S. Jong Jeong, M. Soo Kim, and J. Hyuk Koh, *J. Appl. Phys.* **112**, 124109 (2012).
- ²⁹ R.E. Newnham, D.P. Skinner, and L.E. Cross, *Mater. Res. Bull.* **13**, 525 (1978).

- ³⁰ C. Groh, W. Jo, and J. Rödel, *J. Am. Ceram. Soc.* **97**, 1465 (2014).
- ³¹ C. Groh, D.J. Franzbach, W. Jo, K.G. Webber, J. Kling, L.A. Schmitt, H.J. Kleebe, S.J. Jeong, J.S. Lee, and J. Rödel, *Adv. Funct. Mater.* **24**, 356 (2014).
- ³² A. Ayrikyan, F. Weyland, S. Steiner, M. Duerrschabel, L. Molina-Luna, J. Koruza, and K.G. Webber, *J. Am. Ceram. Soc.* **100**, 3673 (2017).
- ³³ A. Ayrikyan, O. Prach, N.H. Khansur, S. Keller, S. Yasui, M. Itoh, O. Sakata, K. Durst, and K.G. Webber, *Acta Mater.* **148**, 432 (2018).
- ³⁴ A. Ayrikyan, V. Rojas, L. Molina-luna, M. Acosta, J. Koruza, and K.G. Webber, *IEEE Trans. Ultrason. Ferroelectr. Freq. Control* **62**, 997 (2015).
- ³⁵ H. Zhang, C. Groh, Q. Zhang, W. Jo, K.G. Webber, and J. Rödel, *Adv. Electron. Mater.* **1**, 1500018 (2015).
- ³⁶ D. Chen and M. Kamlah, *Rev. Sci. Instrum.* **86**, 113707 (2015).
- ³⁷ V. Segouin, M. Domenjoud, Y. Bernard, and L. Daniel, *J. Eur. Ceram. Soc.* **39**, 2091 (2019).
- ³⁸ W. Jo and J. Rödel, *Appl. Phys. Lett.* **99**, 2012 (2011).
- ³⁹ C.S. Lynch, *Acta Mater.* **44**, 4137 (1996).
- ⁴⁰ X. Tan, J. Frederick, C. Ma, E. Aulbach, M. Marsilius, W. Hong, T. Granzow, W. Jo, and J. Rödel, *Phys. Rev. B - Condens. Matter Mater. Phys.* **81**, 014103 (2010).
- ⁴¹ S. Takasaka, Y. Tsujimi, and T. Yagi, *Phys. Rev. B* **65**, 174102 (2002).
- ⁴² R. Dittmer, W. Jo, J. Rödel, S. Kalinin, and N. Balke, *Adv. Funct. Mater.* **22**, 4208 (2012).
- ⁴³ S.T. Zhang, A.B. Kouna, E. Aulbach, T. Granzow, W. Jo, H.J. Kleebe, and J. Rödel, *J. Appl. Phys.* **103**, 034107 (2008).
- ⁴⁴ C. Xu, D. Lin, and K.W. Kwok, *Solid State Sci.* **10**, 934 (2008).
- ⁴⁵ D.J. Franzbach, *Field Induced Phase Transitions in Ferroelectric Materials*, 2014.
- ⁴⁶ A.B. Kouna Njiwa, E. Aulbach, T. Granzow, and J. Rödel, *Acta Mater.* **55**, 675 (2007).
- ⁴⁷ T. Granzow, T. Leist, A.B. Kouna, E. Aulbach, and J. Rödel, *Appl. Phys. Lett.* **91**, 142904 (2007).
- ⁴⁸ W. Cai, P. Wang, and J. Fan, *Mech. Mater.* **145**, 103391 (2020).
- ⁴⁹ X. Li, G. Chen, X. Chen, G.Q. Lu, L. Wang, and Y.H. Mei, *Solder. Surf. Mt. Technol.* **24**, 120 (2012).
- ⁵⁰ S. Paul, M. Motalab, M.A. Zubaer, and M.Z. Hossain, *J. Adhes. Sci. Technol.* **31**, 1782 (2017).
- ⁵¹ M. Vögler, N. Novak, F.H. Schader, and J. Rödel, *Phys. Rev. B* **95**, 024104 (2017).
- ⁵² R. Dittmer, W. Jo, K.G. Webber, J.L. Jones, and J. Rödel, *J. Appl. Phys.* **115**, 084108 (2014).